Chapter 3

# Elaboration of Nanoporous Copper via Chemical Composition Design of Amorphous Precursor Alloys

Zhenhua Dan, Fengxiang Qin, Izumi Muto, Nobuyoshi Hara and Hui Chang

Additional information is available at the end of the chapter

http://dx.doi.org/10.5772/intechopen.77222

**Abstract**

Au-group (Ag, Au) and Pt-group (Ni, Pd, Pt) metals have lower surface diffusion coefficients than Cu and are defined as LSD. The chemical composition has been designed based on the differences in diffusion coefficients, and the micro-alloying of 1 at % LSD metals with the $Ti_{60}Cu_{40}$ amorphous precursor alloy results in the formation of bi-continuous nanoporous copper (NPC) with finer nanoporous structure. LSD-stabilized NPCs have the smallest characteristic pore sizes of 7 nm and 6 nm after dealloying amorphous $Ti_{60}Cu_{39}Pd_1$ and $Ti_{60}Cu_{39}Pt_1$ precursor alloys, while NPC had a pore size of 39 nm after dealloying the amorphous $Ti_{60}Cu_{40}$ alloy. The refining factor increases approximately from 3.7 for $Ti_{60}Cu_{39}Ag_1$ to 1780 for $Ti_{60}Cu_{39}Pt_1$ precursors due to the dramatic decrease in the surface diffusivity during both preferential dissolution and rearrangement of Cu adatoms. The elaboration efficiencies of $Ti_{60}Cu_{40}$ alloy with addition of 1 at.% Pt-group elements are higher than those of Au-group elements. The homogeneous distribution of LSD elements in both the precursors and final stabilized NPCs played a key role in restriction of the long-distance diffusion of Cu adatoms. LSD-stabilized NPCs are able to have an ultrafine nanoporosity with a pore size almost one order smaller than that from LSD-free alloys.

**Keywords:** amorphous precursor alloys, nanoporous copper, surface diffusion, micro-alloying, elaboration of nanoporous copper

## 1. Introduction

Nanoporous metals (NPMs), a representative type of nanostructured materials, possess intriguing properties to generate promising potentials for various important applications, including catalysis, sensors, actuators, fuel cells, micro-fluidic flow controllers, and

so forth [1–4]. NPMs with a variety of superior physical-chemical properties arisen from their unique pore structure, large specific surface area, and high electrical conductivity have attracted great interests to explore their electrocatalytic properties and greatly extend their potential applications in catalysts, electrochemical sensing, and energy systems [1]. Dealloying primarily originated from the phenomenon of selective corrosion has attracted more attention recently because it has been regarded to be an effective method to fabricate NPMs with a three-dimensional bi-continuous interpenetrating ligament-channel structure at the nanometer scale [5–8]. Nanoporous copper (NPC) is cost-effective and readily fabricated via dealloying process due to the high electrochemical stability. NPCs with different morphologies have been obtained from numerous binary alloy systems including Zn-Cu [7, 9], Mg-Cu [10], Al-Cu [7, 11–16], Ni-Cu [7], Mn-Cu [17, 18], Zr-Cu [19], and Ti-Cu [20].

The characteristic pore sizes of NPCs obtained from the systems mentioned above are relatively larger than those of nanoporous gold (NPG) or nanoporous platinum (NP Pt) and change from few tenth nanometers to few hundredth nanometers, particularly for Zr-Cu system with a pore size of 500 nm [19]. The pore sizes have a significant effect on the mechanical properties of NPMs. The smallest size of nanopores is of order of 3.5 nm for the Cu-Pt system [21]. The yield strength of nanometer-sized NPG ligaments has been improved from ~880 MPa to 4.6 GPa as the NPGs' pore size was refined from 50 nm to 10 nm [22]. As has been reported, the rough NPCs have a relative lower yield strength (i.e., 128 ± 37 MPa with a ligament size of 135 ± 31 nm [17], 86 ± 10 MPa as the ligaments with a size of 300–500 nm of NPCs fabricated by one-step dealloying of the melt-spun Al-50 at.% Cu alloy [11]). It is thus of importance to fabricate NPMs with finer nanostructure with smaller pore size and ligament scales. On the other hand, the elaboration of NPCs is helpful for the enhancements of the catalytic performance and sensitivity for various gaseous phases or metallic ions. Effective ways to reduce the characteristic nanopore sizes have been reported to be dealloying at low temperature [23]; chemical composition design of the precursor alloys, for example, Ag-Au-Pt [24], Al-Pt-Au [25], Ti-Cu-Au [26, 27], Ti-Cu-Ag [28], Ti-Cu-Ni [29], and Ti-Cu-Pd/Pt [30]; and modification of the solution chemistry by using organic acids [31] and by introducing the macromolecules of polyvinylpyrrolidone [32, 33]. The chemical composition design is considered to be an effective way to change the surface diffusion and rearrangements of the adatoms of the noble elements in the precursor alloys since these noble elements take effect from inside to outside. However, the uniform nanoporosity of NPCs is of importance for enhancing the mechanical properties and catalytic performances. Final nanoporous structure is affected by many factors, such as the chemical compositions and initial microstructure of the precursor alloys, the solution chemistries of dealloying solutions, and the experimental conditions (i.e., temperatures, etc.) [12, 34, 35]. The crystalline precursor alloys are extensively dealloyed to prepare NPMs (i.e., coarsen crystalline Al-Cu alloys [11], nanocrystalline Ag-Au, Ag-Au-Pt alloys [22, 24]). While the intermetallic phases or secondary phases exist in the matrix, the final nanoporous structures inherit the characteristics of their initial microstructure of precursor alloys. The characteristics of the casting structures, the intermetallics, and the phase segregations

typical of the crystalline alloys, such as Al-Cu [11–16], Zn-Cu [9], Mg-Cu [10], Mn-Cu [17], Zr-Cu [19], and Ti-Cu [12, 13] alloys are inherited by the final porous structures. The kind and the chemical composition of the initial intermetallic phases and microstructure usually cause the formation of multi-modal nanoporous structures [9–17, 19]. On the contrary, the amorphous alloys exhibit many advantages, especially in their uniform distribution of the alloy constituents without the segregation in the chemical composition and heterogeneity in the microstructure [36]. It is believed that the absence of grain boundary, the large-scaled phase segregations, and intermetallics of amorphous precursors contributes to high uniformity in NPMs. Amorphous alloys with disordered atomic-scale structure, an absence of the weak sites (i.e., grain/phase boundaries typical of crystalline materials) [37], are good to be precursor alloys for the fabrication of the uniform NPMs in some extent. The formation of highly uniform and ultrafine nanoporous structures has been realized for several amorphous alloy systems, including Mg-Cu-Y [31], Ti-Cu-Au [26, 27], Ti-Cu-Ag [28], and Ti-Cu-Ni [29] ternary alloys.

## 2. Materials and methods

On the basis of binary $Ti_{60}Cu_{40}$ alloy, ternary alloys with nominal compositions of $Ti_{60}Cu_{39}M_1$ (M: Ni, Pd, Pt, Ag, Au) were designed and prepared by arc melting of high purity (purity > 99.99 mass%) of raw metals. The LSD elements were divided into two groups: G-I Au-group (Ag, Au) and G-II Pt-group (Ni, Pd, Pt). The surface diffusion coefficients have been reported to be $1.1 \times 10^{-24}$ m $s^{-2}$ for Pd and $3.6 \times 10^{-26}$ m $s^{-2}$ for Pt and $2.2 \times 10^{-23}$ m $s^{-2}$ for Au [38]. The surface diffusion coefficient of Ag in a vacuum is two orders lower than that of Cu as reported [12, 39, 40]. That of Cu is $1.1 \times 10^{-18}$ m $s^{-2}$, more than two orders higher than LSD elements. The surface diffusivity of Ni adatoms in the electrolyte was one tenth of that of Cu adatoms [41]. The ribbon samples were fabricated by melt spinning with a dimension of 20 μm in thickness and 2 mm in width. The starting $Ti_{60}Cu_{39}M_1$ amorphous precursor alloys were treated under the free immersion condition for 43.2 ks in 0.03 M HF solution at 298 K. The detailed information of the experimental procedures has been supplied in the previous publications [27–30]. An X-ray diffractometer (XRD, Rigaku 4200) was employed to identify the change in the lattice constants, crystalline states of dealloyed alloys and microstructure of precursor alloys and dealloyed alloys. The porous morphologies of the nanoporous NPC and LSD-stabilized samples were observed by a scanning electron microscope (JEOL, JIB-4610F). The chemical composition of the as-dealloyed samples was analyzed by an energy dispersive X-ray spectroscope (JEOL, JIB-4610F). Transmission electron microscopes (JEOL, HC2100, and ARM200) were used to observe the internal porous structure, the nanoporosity of dealloyed alloys, and crystalline characteristics of the LSD-stabilized Cu ligaments in high-resolution TEM modes. The nanoporosity was mainly analyzed on the basis of the average size of the nanopores and ligaments. The characteristic pore size of as-dealloyed alloys was confirmed by the single chord method for over 125 sites on SEM and TEM images.

## 3. Elaboration of nanoporous copper via the chemical composition design

### 3.1. Characteristics of LSD-added Ti-Cu precursor alloys and nanoporous counterparts

The XRD patterns of the as-spun $Ti_{60}Cu_{40}$, $Ti_{60}Cu_{39}Ni_1$, $Ti_{60}Cu_{39}Pd_1$, and $Ti_{60}Cu_{39}Pt_1$ ribbons present one strong and broad diffraction peak at 41° and a weak diffraction peak at 70–75°, indicating an amorphous structure, as shown in **Figure 1**. Other LSD-substituted $Ti_{60}Cu_{40}$ precursor alloys were still amorphous states, indicating that the micro-alloying of 1 at.% LSD elements had not generated the heterogeneous microstructure or phase segregation. The high-resolution TEM images (HRTEM) and corresponding selective area diffraction patterns (SADP) of as-spun $Ti_{60}Cu_{40}$ and $Ti_{60}Cu_{39}M_1$ show that as-spun LSD-substituted $Ti_{60}Cu_{39}M_1$ alloys had an amorphous structure without the crystalline clusters and phase segregations [27]. As is well known, because G-I LSD elements, Ag and Au, have a similar crystal structure to Cu, the addition of minor amounts of G-I elements has thus no significant influence on the structure of as-spun alloys [26, 27]. In G-II elements, Ni, Pd, and Pt, three strong diffraction peaks were observed in the XRD patterns of the dealloyed $Ti_{60}Cu_{39}Pd_1$ and $Ti_{60}Cu_{39}Pt_1$ ribbons after dealloying for 43.2 ks in the 0.03 M HF solution. The diffraction peaks were identified to be *fcc* Cu and had slightly shifted to low diffraction angles due to the expansion of the LSD-substituted

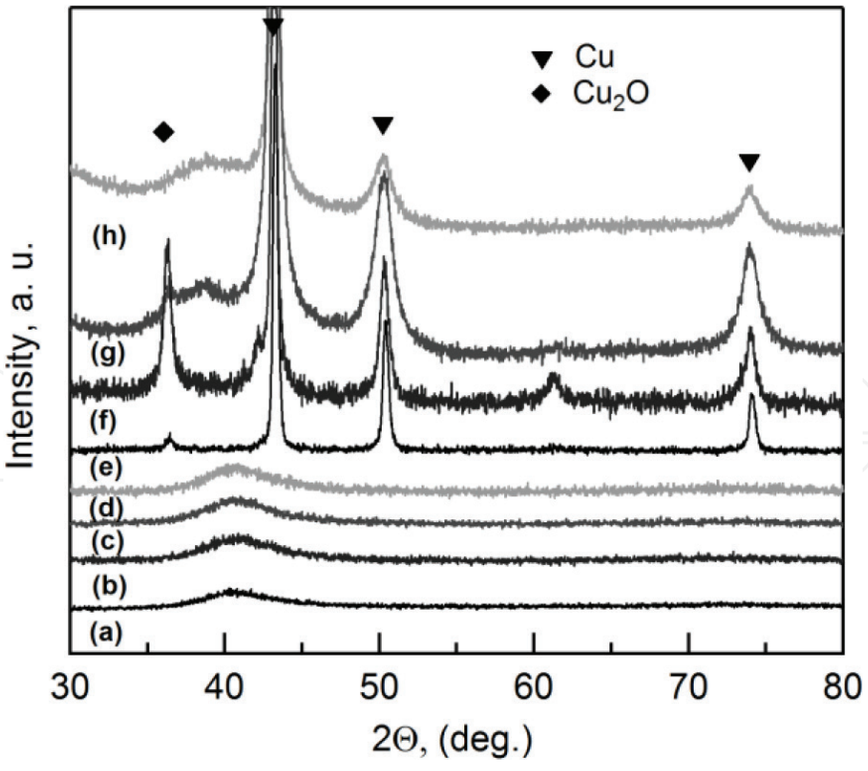


**Figure 1.** XRD patterns of as-spun (a, b, c, d) and dealloyed (e, f, g, h) $Ti_{60}Cu_{40}$ (a, e), $Ti_{60}Cu_{39}Ni_1$ (b, f), $Ti_{60}Cu_{39}Pd_1$ (c, g), and $Ti_{60}Cu_{39}Pt_1$ (d, h) ribbons after immersion in 0.03 M HF solution for 43.2 ks. Reproduced with permission from Dan et al. [30] Copyright Materials Transactions.

http://dx.doi.org/10.5772/intechopen.77222

unit cells. The small peak around 36° was considered to be from the $Cu_2O$ phase. The absence of strong diffraction peaks from crystalline Pd and Pt phases indicates that CuPd or CuPt solid solution formed after dealloying. These XRD patterns were similar to those of Ag-, Au-, and Ni-stabilized NPCs [26–29]. **Figure 2** shows the change in the lattice constant, $\alpha$, and the grain sizes, $L$, with 1 at% addition of Au-group (G-I) and Pt-group (G-II). The standard lattice constants are reported to be 0.3524 nm for Ni, 0.3608 nm for Cu, 0.3891 nm for Pd, 0.3924 nm for Pt, 0.4078 nm for Au, and 0.4085 nm for Ag, respectively. The lattice constants of NPCs were estimated to be 0.3615–0.3627 nm on the basis of the XRD data of Cu (111) peaks. The lattice constants became larger when the added elements had larger lattice constants except in the case of Ag. As indicated in **Figure 2**, the Cu lattice expanded more when Pd and Pt were micro-alloyed into the $Ti_{60}Cu_{40}$ alloy. The added Ni, Pd, or Pt atoms were thus considered to substitute the Cu atoms in the Cu lattice to a higher extent than in the Ag- or Au-added cases, resulting in the expansion of the Cu lattice constants from 0.3615 nm to 0.3627 nm in **Figure 2**. In previous works it was found that the Au or Ag phase was formed after dealloying the $Ti_{60}Cu_{39}Au_1$ and $Ti_{60}Cu_{39}Au_1$ precursor alloys [26–29]. The absence of diffraction peaks from the Pd or Pt phase in the XRD patterns of dealloyed $Ti_{60}Cu_{39}Pd_1$ and $Ti_{60}Cu_{39}Pt_1$ ribbons and the large expansion of the lattice constants of the NPCs indicated that more Pt-group atoms invaded the Cu lattice than Au-group atoms (i.e., Ag addition and Au addition) for NPCs from precursor alloys micro-alloyed with LSD elements [26–29]. On the other hand, the grain sizes were reduced to 15 nm and 13 nm when the Pd and Pt were added into $Ti_{60}Cu_{40}$ ribbons.

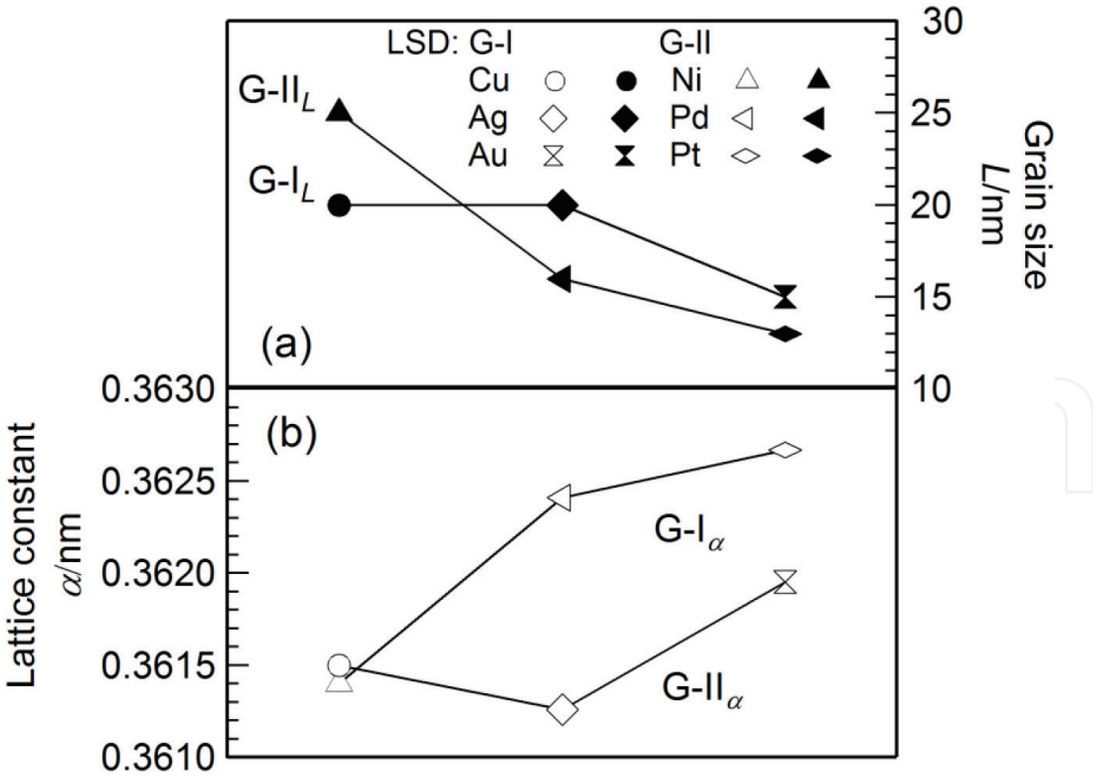


**Figure 2.** Dependence of the grain sizes (a) and the lattice constants (b) of dealloyed $Ti_{60}Cu_{39}M_1$ (M: LSD—G-I Cu, Ag, and Au and G-II Ni, Pd, and Pt) ribbons on the addition of the elements. The lines are used for view guide of data points in G-I and G-II. Reproduced with permission from Dan et al. [30] Copyright Materials Transactions.

The decrease in the grain sizes was considered to be due to the retardation of the self-diffusion of Cu adatoms by LSD elements [27, 29, 30]. The diffusion distance of Cu adatoms under free diffusion patterns is prevailed in a long-distance diffusion mode [2, 5, 10, 19–21]. However, the long-distance self-diffusion of Cu adatoms was interrupted and restricted by the LSD adatoms during the rearrangement of adatoms and resulted in an accumulation of Cu and LSD adatoms in a smaller scale. Consequently, smaller grains were formed when the Pt-group elements (Pd, Pt) and Au element were used to stabilize NPCs.

The nanoporous surface morphologies of dealloyed $Ti_{60}Cu_{39}M_1$ (M: Cu, Ag, Au, Ni, Pd, Pt) alloys are shown in **Figure 3**. The mean pore size of the nanoporous structure of as-dealloyed $Ti_{60}Cu_{40}$ ribbons was about 71 nm after dealloying in 0.03 M HF solution. The characteristic length scales of ligaments of NPC obtained from $Ti_{60}Cu_{40}$ alloy were 74 nm in 0.03 M HF solution. The characteristic sizes for the nanopores and ligaments were confirmed to be for 41 and 48 nm for dealloyed $Ti_{60}Cu_{39}Ag_1$ precursor, 16 nm and 27 nm for $Ti_{60}Cu_{39}Au_1$ precursor, 12 nm and 26 nm for $Ti_{60}Cu_{39}Ni_1$ precursor, 9 nm and 24 nm for $Ti_{60}Cu_{39}Pd_1$ precursor, and 8.5 nm and 31 nm for $Ti_{60}Cu_{39}Pt_1$ precursor. **Figure 4** shows a typical bright field TEM image (BFI), their corresponding selected area diffraction pattern (SADP) of $Ti_{60}Cu_{39}M_1$ (M: Cu, Ag, Au, Ni, Pd, Pt) amorphous alloys after dealloying for 43.2 ks. A bi-continuous porous microstructure was formed with a characteristic pore size of 7 nm for the dealloyed $Ti_{60}Cu_{39}Pd_1$ ribbon and ca. 6 nm for the dealloyed $Ti_{60}Cu_{39}Pt_1$ ribbon, respectively (**Figure 4e** and **3f**). The diffraction rings in the SAD patterns were assigned to Cu (111), (200), (220), and (311) (JCPDS

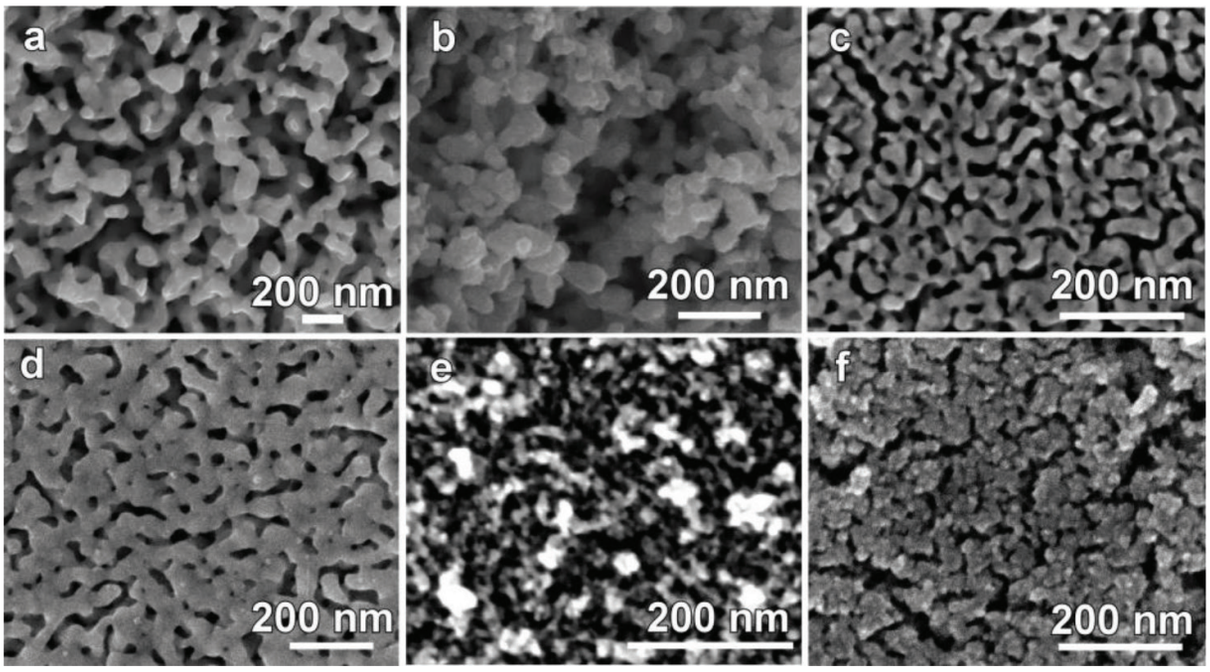


**Figure 3.** Typical surface morphologies of dealloyed $Ti_{60}Cu_{40}$ (a), $Ti_{60}Cu_{39}Ag_1$ (b), $Ti_{60}Cu_{39}Au_1$ (c), $Ti_{60}Cu_{39}Ni_1$ (d),$Ti_{60}Cu_{39}Pd_1$ (e), and $Ti_{60}Cu_{39}Pt_1$ (f) precursors after dealloying in 0.03 M HF solution for 43.2 ks. Reproduced with permission from Dan et al. [30] Copyright Materials Transactions. Reproduced with permission from Dan et al. [27, 30] copyright Elsevier and Materials Transactions.

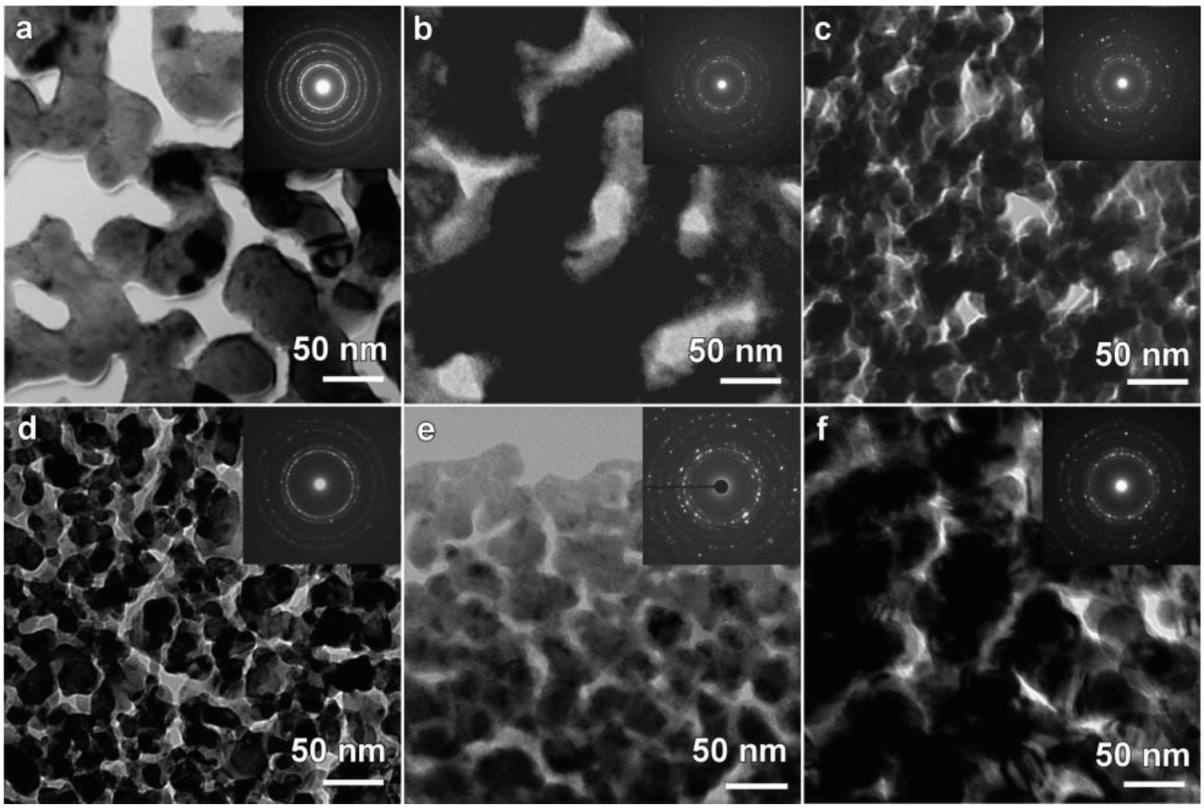


**Figure 4.** Typical bright field TEM images of dealloyed $Ti_{60}Cu_{40}$ (a), $Ti_{60}Cu_{39}Ag_1$ (b), $Ti_{60}Cu_{39}Au_1$ (c), $Ti_{60}Cu_{39}Ni_1$ (d),$Ti_{60}Cu_{39}Pd_1$ (e), and $Ti_{60}Cu_{39}Pt_1$ (f) precursors after dealloying in 0.03 M HF solution for 43.2 ks. The insets are their corresponding selected area diffraction patterns. Reproduced with permission from Dan et al. [30] Copyright Materials Transactions.

card No. 02-1225), and the inner ring was done for $Cu_2O$ (111) (JCPDS card No. 74-1230). The diffraction rings from the $Cu_2O$ phase were absent in the inset SADP in **Figure 4e**. The ligament sizes were confirmed to be ca. 23 nm for the dealloyed $Ti_{60}Cu_{39}Pd_1$ ribbon and ca. 30 nm for the dealloyed $Ti_{60}Cu_{39}Pt_1$ ribbon. The BFI images mainly reflected the internal nanoporous structures with a finer porosity in comparison to those in the surface regions. It is considered that the finer nanoporous structure in the internal parts mainly resulted from the lower concentration gradients inside the channels. As shown in **Figure 4e** and **f**, the pore size of Pd-stabilized and Pt-stabilized NPCs had a mean pore size of 7 and 6 nm, respectively. As shown in **Figure 4b–d**, the characteristic pore size of NPCs stabilized by the micro-alloying of Ni, Ag, and Au [27–29] has been reported to be 11 nm, 28 nm, and 12 nm on the basis of TEM analysis, respectively. The mean pore size of dealloyed $Ti_{60}Cu_{40}$ ribbons confirmed by TEM observation was 39 nm in **Figure 4a** [20]. The pore size decreased more than one order due to the addition of either Pd or Pt as shown in **Figure 4e** and **f**. The characteristic scale length of the nanopores and ligaments of dealloyed $Ti_{60}Cu_{39}Pd_1$ and $Ti_{60}Cu_{39}Pt_1$ ribbons decreased dramatically. On the basis of XRD, TEM, and SEM-EDX analysis, the residue is considered to be *fcc* CuPd and *fcc* CuPt solid solution. The similarity existed in all LSD-substituted $Ti_{60}Cu_{39}M_1$ (M: Ag, Au, Ni, Pd, Pt). Commonly the Cu(LSD) solid solutions can be regarded as the residual phases after dealloying. However, the selective dissolution is slightly different which caused

the formation of Ag and Au phases [27, 28]. Although NPCs from $Ti_{60}Cu_{39}Ag_1$ precursor had a large final nanopore, the elaborating behavior still happened at the initial dealloying stages with a high refining efficiency [28]. As shown in **Figure 5**, the distribution of Au LSD element was profiled. The uniform distribution of Au elements can be confirmed here. For other precursor alloys, the residual LSD elements had similar profiles which benefited from the uniform distribution of these LSDs in the amorphous precursor alloys.

### 3.2. Effects of LSDs on surface diffusion

On the basis of the surface diffusion-controlled coarsening mechanism, the surface diffusivity, $D_s$, at various dealloying temperatures was estimated by the equation [42]:

$$D_s = \frac{[\,d(t)\,]^4 kT}{32\gamma t\, a^4} \tag{1}$$

where $k$ is Boltzmann constant ($1.3806 \times 10^{-23}$ J $K^{-1}$), $\gamma$ is surface energy, $t$ is the dealloying time (43,200 s), $d(t)$ is the pore size at $t$, $T$ is the temperature, and $\alpha$ is the lattice constant. The pore size of NPCs confirmed by TEM micrographs and lattice constants calculated from XRD data were adopted for calculation of $D_s$. The surface energy of Cu has been reported to be 1.79 J $m^{-2}$ [40, 43]. The surface energy of micro-alloyed elements has been reported to be 1.24 J $m^{-2}$ for Ag, 1.50 J $m^{-2}$ for Au, 2.0 J $m^{-2}$ for Ni, 2.0 J $m^{-2}$ for Pd, and 2.49 J $m^{-2}$ for Pt [40, 43]. The concentration of Au-group elements (Ag, Au) and Pt-group elements (Ni, Pd, Pt) in the precursor alloys was 1 at%. The concentration of added elements (Ag, Au, Ni, Pd, Pt) in NPCs after dealloying should theoretically be 2.5 at% if the dissolution of Cu in HF solution is not considered. Therefore, the surface energy of LSD-stabilized NPCs is considered to be very close to that of Cu. The surface energy of Cu, 1.79 J $m^{-2}$, was adopted for the calculation of $D_s$. The characteristic nanopore sizes were summarized in **Figure 6a**, which has been illustrated above. On the other hand, the surface diffusivities of these LSD-stabilized alloys in 0.03 M HF solutions

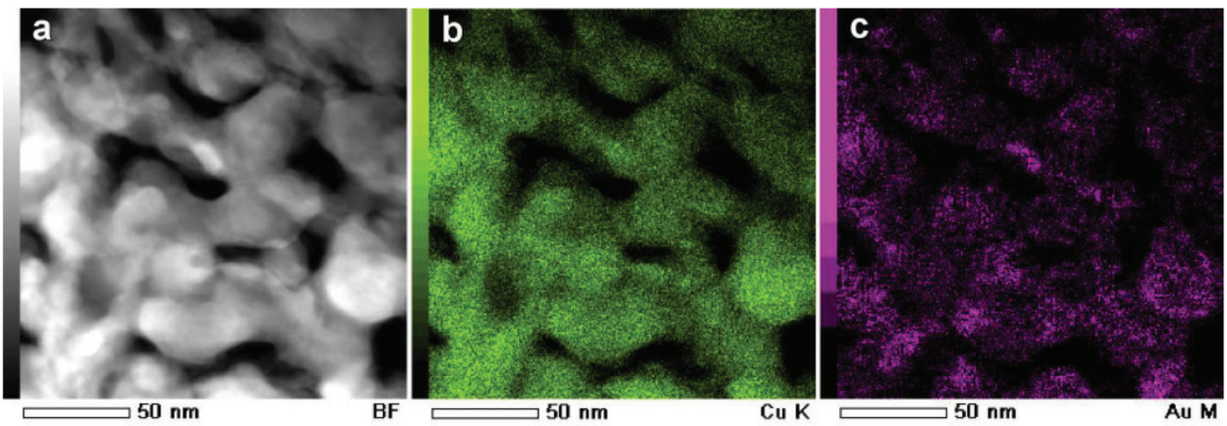


**Figure 5.** High-angle annular dark field scanning TEM image (a) and elemental mapping of Cu (b) and Au (c) of dealloyed $Ti_{60}Cu_{39}Au_1$ precursors after dealloying in 0.03 M HF solution for 43.2 ks. Reproduced with permission from Dan et al. [27] Copyright Elsevier.

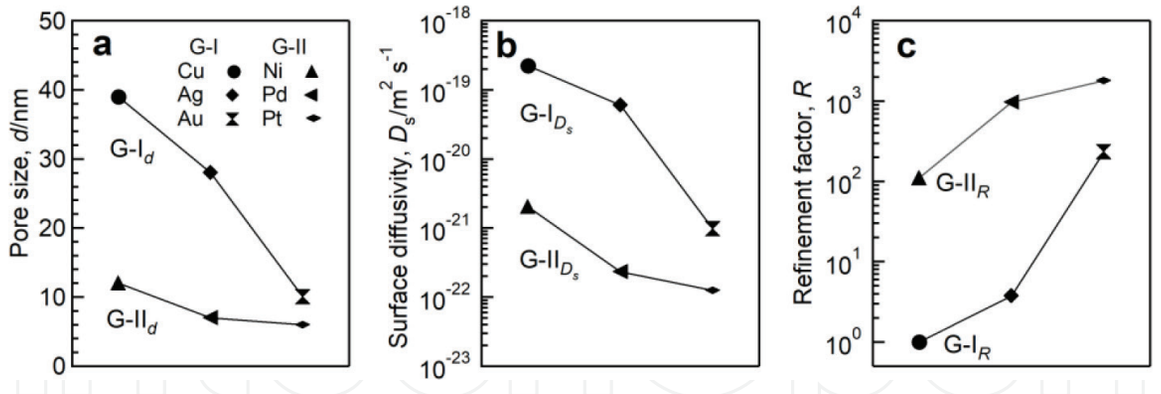


**Figure 6.** Mean pore size (a), surface diffusivity (b), and refining factor of dealloyed $Ti_{60}Cu_{39}M_1$. M is the selected LSD elements including Ag, Au, Ni, Pd, and Pt. The lines are used for view guide of data points in G-I and G-II. Reproduced with permission from Dan et al. [30] Copyright Materials Transactions.

can be modified. As shown in **Figure 5b**, the value of $D_s$ was estimated to be $2.5 \times 10^{-18}$ m$^2$ s$^{-1}$ for $Ti_{60}Cu_{40}$ ribbon, $6.0 \times 10^{-20}$ m$^2$ s$^{-1}$ for $Ti_{60}Cu_{40}$ ribbon, $9.7 \times 10^{-21}$ m$^2$ s$^{-1}$ for $Ti_{60}Cu_{39}Au_1$ ribbon and $2.0 \times 10^{-21}$ m$^2$ s$^{-1}$ for $Ti_{60}Cu_{39}Ni_1$ ribbon, $2.3 \times 10^{-22}$ m$^2$ s$^{-1}$ for $Ti_{60}Cu_{39}Pd_1$ ribbon, and $1.3 \times 10^{-22}$ m$^2$ s$^{-1}$ for $Ti_{60}Cu_{39}Pt_1$ ribbon, respectively. The surface diffusivity decreased more than four orders of magnitude due to the addition of Pd and Pt. Compared with $D_s$ of the Au-group-stabilized NPCs, the decrease in $D_s$ in the Pt-group-stabilized NPCs was remarkable.

The refining factor, $R$, is defined as the ratio between the surface diffusivity, $D_s$, of NPC obtained from amorphous $Ti_{60}Cu_{40}$ precursor (numerator) and NPCs stabilized by LSDs (denominator):

$$R = \frac{D_s^{Cu}}{D_s^{L}} \approx \frac{[d(t)^{Cu}]^4}{[d(t)^{L}]^4} \times \frac{[a^{Cu}]^4}{[a^{L}]^4} \tag{2}$$

As shown in **Figure 6c**, the estimated refining factor was 968 for $Ti_{60}Cu_{39}Pd_1$ ribbon and 1780 for $Ti_{60}Cu_{39}Pt_1$ ribbon, respectively. In other cases, the value of $R$ changed from 4 for the dealloyed $Ti_{60}Cu_{39}Ag_1$ ribbon, 111 for the dealloyed $Ti_{60}Cu_{39}Ni_1$ ribbon, and 231 for the dealloyed $Ti_{60}Cu_{39}Au_1$ ribbon, respectively. The refining efficiency of the micro-alloying of the Pt-group elements into the precursor $Ti_{60}Cu_{40}$ alloy was one order higher than that of the Au-group cases. The lower value of $R$ for $Ti_{60}Cu_{40}$ alloy stabilized by Au-group (G-I) elements could take into account from several aspects: (1) the larger self-diffusion coefficients of Ag and Au than that of Cu [44–48] and (2) the large misfit in the atomic radii [49]. As has been reported before [44–48], the self-diffusion coefficients of Au- and Pt-group elements are ranked as following: Ag > Cu > Au > Ni > Pd > Pt. As such, there are more possibilities for Ag adatoms to meet with other Ag adatoms during the diffusion and rearrangements processes of dealloying to form clusters and to develop the Ag phase because it has a larger self-diffusion coefficient than Cu atoms [44, 48]. The self-diffusion coefficient of Au is slightly smaller than that of Cu [45]. Because the misfit in the atomic radius between Cu and Ag and Cu and Au is about 13%, the incorporation of Ag-Au atoms into the Cu lattice becomes more difficult than that of Cu/Cu atoms. On the other hand, the self-diffusion coefficients of Pt-group (G-II)

elements are more than two orders lower than that of Cu element [47, 48], and the formation of the crystalline phase of G-II elements (Ni, Pd, Pt) was interrupted by the fast diffusion of Cu adatoms. Furthermore, the misfits in the atomic radius between Cu and Pd and Pt elements are ca. 8%, and the incorporation of Pd/Pt into the Cu lattices appears more easily. The changes in the lattice constants of the NPCs stabilized by G-I and G-II indicated by XRD patterns in **Figure 1** and Refs. [27, 28] support the present hypothesis. As has presented above, the formation of the Ag and Au crystalline phases after dealloying is considered to be due to the difference in self-diffusion behaviors and misfits of the atomic radius. The minor addition of Group-I LSDs causes the formation of the crystalline Ag/Au phases, and the refining factors of Group I were small. On the other hand, the micro-alloying by Group-II LSDs mainly resulted in the invasion of the Cu lattices, with some Cu atoms in the lattice substituted by Ni, Pd, and Pt atoms, forming solid solutions, and the refining factors for Group II were high. In some extent, these LSD atoms in the lattice are considered to be the main contributors for the elaboration of NPCs.

The diffusion in the interfacial regions between Cu, LSD adatoms, and Ti adatoms played a key role in the formation of ultrafine NPCs. For example, Evangelakis investigated the diffusion of Au adatoms on Cu and self-diffusion of Cu adatoms by using the molecular dynamic method [50]. They have found that diffusion of Cu adatoms takes place exclusively by hopping from one adatom position to an adjacent one and that multiple jumps are frequent at low temperatures. On the other hand, Au adatoms on the NPC ligaments hopped less frequently than in the case of Cu self-diffusion. The migration energy required for hopping of Au on Cu was almost twice that of the corresponding energy for Cu adatoms. While the diffusion of Au on Cu was more difficult than the diffusion of Cu on Cu, this phenomenon is compatible with the binding energy of Au adatoms, which is found to be 2.77 eV for Au adatoms and 2.26 eV for Cu adatoms. The Au adatoms relaxed at a distance −15% smaller than the bulk interlayer distance, but in the case of the Cu adatoms, it was −10% for the same quantity [50]. The Cu adatoms diffused quickly in and out by themselves; however, the Au adatoms at the activated sites diffused out slowly and hardly ever diffused back to the NPC ligaments. Consequently, Au adatoms gradually accumulated outside the ligaments during the dealloying [27, 30]. As a result, Au adatoms uniformly distributed outside the ligaments after dealloying for 43.2 ks via the hopping mechanism, as shown in **Figure 5**. When more Au was added to TiCu amorphous alloys, the surface coverage of Au adatoms increased during dealloying, suggesting that the accumulation rate of Au adatoms in the more concentrated solutions was higher due to the faster migration of Au and Cu adatoms [27]. Because the accumulated Au adatoms built up a continuous outmost diffusion barrier, the behaviors of diffusion and rearrangements of Cu and Au adatoms can be fulfilled to form ultrafine NPCs from both the LSD-substituted $Ti_{60}Cu_{40}$ amorphous precursor alloys in HF solutions. The diffusion behavior for other LSD-stabilized nanoporous structures was considered to be similar. However, the accumulation of G-II Pt-group elements (Ni, Pd, and Pt) with much slower diffusion rates and Ni, Pd, and Pt cluster or grains with much smaller size less than 7 nm tended to form, which are not sensitive to X-ray [51]. As has been reported [52], a bimodal nanoporous structure with a pore size of 10 nm and 20 nm has been fabricated from $Al_{75}Pd_{17.5}Au_{7.5}$ precursor alloys by successive dealloying. The initial heterogeneous microstructure consisting of $Al_2Au$- and $Al_3Pd$-type intermetallics causes the formation of a bimodal nanoporous structure. The similar evolution of bimodal or multimodal nanoporosity on precursor alloys heterogeneous in microstructure

has been reported [11, 12, 14, 20, 41]. Amorphous precursor alloys with homogeneously distributed Cu, Ti, and LSD atoms also have an important refining effect. The uniform distribution of added Pd and Pt atoms in final NPCs resulted in smaller nanopores, as shown in **Figures 3** and **4**. In 2008, fine nanoporous AuPt alloys with a pore size of about 5 nm were fabricated from an $Ag_{65}Au_{29}Pt_6$ precursor [24]. The alloying of 6 at% Pt into the $Ag_{65}Au_{35}$ alloy effectively reduced the pore size from 10 to 20 nm to about 4 nm, which also supports the present results. However, the high cost of Au and Pt weakens their potential application. By minor addition of the 1 at% Pt-group elements, it is possible to elaborate NPCs down to a pore size of approximately 6 nm, comparable to high-cost AuPt nanoporous in nanoporosity. So far the LSD-stabilized NPCs had a relative small nanopores and narrow ligaments comparable to these of NP Au, NP Pd, and NP Pt. If catalytic Au, Pd, or Pt monolayer is electrodeposited on ultrafine NPCs, the catalytic performance of this kind of cost-effective porous materials is able to be close to those Au, Pd, or Pt catalysts. Meanwhile, if the oxides are assembled on ultrafine NPC templates, the new-developed nanocomposites can be used as promising pseudocapacitors to contribute in the energy conversion fields.

## 4. Conclusions

The 1 at% minor addition of low surface diffusive (LSD) elements in two groups (G-I, Au-group (Ag, Au), and G-II, Pt-group (Ni, Pd, Pt)) is able to elaborate the nanoporous Cu structure dealloyed from micro-alloyed $Ti_{60}Cu_{40}$ alloy efficiently. The chemical compositions of $Ti_{60}Cu_{40}$ alloys stabilized by the addition of G-II metals were shown to be more effective in refining nanoporous structure than the addition of G-I metals. Nanoporous Cu with a pore size of less than 7 nm was obtained from $Ti_{60}Cu_{39}Pd_1$ and $Ti_{60}Cu_{39}Pt_1$ ribbons after dealloying. The residue of dealloyed $Ti_{60}Cu_{39}Pd_1$ and $Ti_{60}Cu_{39}Pt_1$ ribbons was confirmed to be bimetallic solid solutions, such as fcc Cu(Pd) or Cu(Pt) solid solutions, and fcc Cu(Au), Cu(Ag), and Cu(Ni) solid solutions formed after dealloying. The refining factor increases approximately from 3.7 for the $Ti_{60}Cu_{39}Ag_1$ precursor alloy to 1780 for the $Ti_{60}Cu_{39}Pt_1$ precursor alloy. The elaboration was attributed to the dramatic decrease in the surface diffusivity during both preferential dissolution and rearrangement of Cu adatoms. The refinement efficiency of the micro-alloying of the G-II LSDs in Pt-group elements was almost one order higher than that of the G-I LSDs in Au-group elements. The homogeneous distribution of LSD elements in both of the amorphous precursor alloys and the final stabilized NPCs played a key role in refining the NPCs. The strategy outlined in this work has the potential to be applied to other alloy systems to obtain other ultrafine nanoporous metals with comparable nanoporosity to those high-cost catalysts.

## Acknowledgements

The authors gratefully acknowledge the financial support from the Ministry of Education, Culture, Sports, Science, and Technology (MEXT) Japan through Grant-In-Aid for Science Research in a Priority Area on “Research and Development Project on Advanced Materials Development and Integration of Novel Structured Metallic and Inorganic Materials” and a

Grant-in-Aid for Young Scientists (B) under Grant No. 24760567. This work is also financially supported by the Natural Science Foundation of China under Grant no. 51671106 and Natural Science Foundation of Jiangsu Province under Grants nos. BK20171424 and BK20151536. The authors would also like to acknowledge Jiangsu Collaborative Innovation Center for Advanced Inorganic Function Composites, the International S&T Cooperation Program of China (2015DFA51430).

## Conflict of interest

The authors declare no conflict of interest.

## Author details

Zhenhua Dan[1,2]*, Fengxiang Qin[3], Izumi Muto[2], Nobuyoshi Hara[2] and Hui Chang[1]

*Address all correspondence to: zhenhuadan@njtech.edu.cn

1 Tech Institute for Advanced Materials and College of Materials Science and Engineering, Nanjing Tech University, Nanjing, China

2 Department of Materials Science, Tohoku University, Sendai, Japan

3 School of Materials Science and Engineering, Nanjing University of Science and Technology, Nanjing, China

## References

[1] Zhang JT, Li CM. Nanoporous metals: Fabrication strategies and advanced electrochemical applications in catalysis, sensing and energy systems. Chemical Society Review. 2012;**41**:7016-7031. DOI: 10.1039/C2CS35210A

[2] You TY, Niwa O, Tomita M, Hirono S. Characterization of platinum nanoparticle-embedded carbon film electrode and its detection of hydrogen peroxide. Analytical Chemistry. 2003;**75**:2080-2085. DOI: 10.1021/ac026337w

[3] Weissmueller J, Viswanath RN, Kramer D, Zimmer P, Wuerschum R, Gleiter H. Charge-induced reversible strain in a metal. Science. 2003;**300**:312-315. DOI: 10.1126/science.1081024

[4] Joo SH, Choi SJ, Oh I, Kwak J, Liu Z, Terasaki O, Rvoo R. Ordered nanoporous arrays of carbon supporting high dispersions of platinum nanoparticles. Nature. 2001;**412**:169-172. DOI: 10.1038/35084046

[5] Forty AJ. Corrosion micromorphology of noble metal alloys and depletion gliding. Nature. 1979;**282**:597-598. DOI: 10.1038/282597a0

[6] Dursun A, Pugh DV, Corcoran SG. Dealloying of ag-au in halide-containing electrolytes: Affect on critical potential and pore size. Journal of The Electrochemical Society. 2003;**150**:B355-B360. DOI: 10.1149/1.1580824

[7] Pryor MJ, Fister JC. The mechanism of dealloying of copper solid solutions and intermetallics phases. Journal of the Electrochemical Society. 1984;**131**:1230-1235. DOI: 10.1149/1.2115793

[8] Liu HT, He P, Li ZY, Li JH. High surface area nanoporous platinum: Facile fabrication and electrocatalytic activity. Nanotechnology. 2006;**17**:2167-2173. DOI: 10.1088/0957-4484/17/9/015/meta

[9] Pickering HW. Formation of new phase during anodic dissolution of Zn-rich cu-Zn alloys. Journal of the Electrochemical Society. 1970;**117**:8-15. DOI: 10.1149/1.2407450

[10] Zhao CC, Qi Z, Wang XG, Zhang ZH. Fabrication and characterization of monolithic nanoporous copper through chemical dealloying of Mg-Cu alloys. Corrosion Science. 2009;**51**:2120-2125. DOI: 10.1016/j.corsci.2009.05.043

[11] Qi Z, Zhao CC, Wang XG, Lin JK, Shao W, Zhang ZH, Bian XF. Formation and characterization of monolithic nanoporous copper by chemical dealloying of Al-Cu alloys. The Journal of Physical Chemistry C. 2009;**113**:6694-6698. DOI: 10.1021/jp810742z

[12] Zhang ZH, Wang Y, Qi Z, Zhang WH, Qin JY, Frenzel J. Generalized fabrication of nanoporous metals (Au, Pd, Pt, Ag and Cu) through chemical dealloying. Journal of Physical Chemistry C. 2009;**113**:12629-12636. DOI: 10.1021/jp811445a

[13] Liu WB, Zhang SC, Li N, Zheng JW, Xing YL. A facile one-pot route to fabricate nanoporous copper with controlled hierarchical pore size distributions through chemical dealloying of Al-Cu alloy in an alkaline solution. Microporous and Mesoporous Materials. 2011;**138**:1-7. DOI: 10.1016/j.micromeso.2010.10.003

[14] Liu WB, Zhang SC, Li N, Zheng JW, Xing YL. Microstructure evolution of monolithic nanoporous copper from dual-phase Al 35 atom% Cu alloy. Journal of the Electrochemical Society. 2010;**157**:D666-D670. DOI: 10.1149/1.3497308

[15] Liu WB, Zhang SC, Li N, Zheng JW, Xing YL. Dealloying behaviour of dual-phase Al 40 atom % Cu alloy in an alkaline solution. Journal of the Electrochemical Society. 2011;**158**:D91-D94. DOI: 10.1149/1.3511771

[16] Liu WB, Zhang SC, Li N, Zheng JW, Xing YL. Influence of phase constituent and proportion in initial Al-Cu alloys on formation of monolithic nanoporous copper through chemical dealloying in an alkaline solution. Corrosion Science. 2011;**53**:809-814. DOI: 10.1016 /j.corsci.2010.11.017

[17] Hayes JR, Hodge AM, Biener J, Hamza AV. Monolithic nanoporous copper by dealloying Mn-Cu. Journal of Materials Research. 2006;**21**:2611-2616. DOI: 10.1557/jmr.2006.0322

[18] Chen LY, Yu JS, Fujita T, Chen MW. Nanoporous copper with tunable nanoporosity for SERS applications. Advanced Functional Materials. 2009;**19**:1221-1226. DOI: 10.1002/adfm.200801239

[19] Lu HB, Li Y, Wang FH. Synthesis of porous copper from nanocrystalline two-phase Cu-Zr film by dealloying. Scripta Materialia. 2007;**56**:165-168. DOI: 10.1016/j.scriptamat.2006.09.009

[20] Dan ZH, Qin FX, Sugawara Y, Muto I, Hara N. Fabrication of nanoporous copper by dealloying amorphous binary Ti-Cu alloys in hydrofluoric acid solutions. Intermetallics. 2012;**29**:14-20. DOI: 10.1016/j.intermet.2012.04.016

[21] Pugh DV, Dursun A, Corcoran SG. Formation of nanoporous platinum by selective dissolution of Cu from $Cu_{0.75}Pt_{0.25}$. Journal of Materials Research. 2003;**18**:216-221. DOI: 10.1557/JMR.2003.0030

[22] Biener J, Hodge AM, Hayes JR, Volkert CA, Zepeda-Ruiz LA, Hamza AV, Abraham FF. Size effects on the mechanical behavior of nanoporous Au. Nano Letters. 2006;**6**:2379-2382. DOI: 10.1021/nl061978i

[23] Qian LH, Chen MW. Ultrafine nanoporous gold by low-temperature dealloying and kinetics of nanopore formation. Applied Physics Letters. 2007;**91**:083105. DOI: 10.1063/1.2773757

[24] Snyder J, Asanithi P, Dalton AB, Erlebacher J. Stabilized nanoporous metals by dealloying ternary alloy precursors. Advanced Materials. 2008;**20**:4883-4886. DOI: 10.1002/adma.200702760

[25] Sun JZ, Yan XJ, Zhao BG, Liu L, Gao YL, Zhang ZH. Modulation of compositions and electrocatalytic activities of quaternary nanoporous Pt-based alloys via controllable dealloying. International Journal of Hydrogen Energy. 2016;**41**:9476-9489. DOI: 10.1016/j.ijhydene.2016.04.098

[26] Dan ZH, Qin FX, Sugawara Y, Muto I, Hara N. Dependency of the formation of Au-stabilized nanoporous copper on the dealloying temperature. Microporous and Mesoporous Materials. 2014;**186**:181-186. DOI: 10.1016/j.micromeso.2013.12.003

[27] Dan ZH, Qin FX, Sugawara Y, Muto I, Hara N. Elaboration of nanoporous copper by modifying surface diffusivity by the minor addition of gold. Microporous and Mesoporous Materials. 2013;**165**:257-264. DOI: 10.1016/j.micromeso.2012.08.026

[28] Dan ZH, Qin FX, Makino A, Sugawara Y, Muto I, Hara N. Fabrication of nanoporous copper by dealloying of amorphous Ti-Cu-Ag alloys. Journal of Alloys and Compounds. 2014;**586**:S134-S138. DOI: 10.1016/j.jallcom.2013.01.087

[29] Dan ZH, Qin FX, Sugawara Y, Muto I, Makino A, Hara N. Nickel-stabilized nanoporous copper fabricated from ternary TiCuNi amorphous alloys. Materials Letters. 2013;**94**:128-131. DOI: 10.1016/j.matlet.2012.12.028

[30] Dan ZH, Qin FX, Hara N. Refinement of Nanoporous copper: A summary of micro-alloying of Au-group and Pt-group elements. Materials Transactions. 2014;**55**:796-800. DOI: 10.2320/matertrans.M2013445

[31] Qin FX, Dan ZH, Hara N, Li WR, Li YD. Selective dissolution of an amorphous $Mg_{65}Cu_{25}Y_{10}$ alloy in organic acids and dilute HCl solution. Materials Chemistry and Physics. 2016;**179**:27-34. DOI: 10.1016/j.matchemphys.2016.05.001

[32] Dan ZH, Qin FX, Hara N. Polyvinylpyrrolidone macromolecules function as a diffusion barrier during dealloying. Materials Chemistry and Physics. 2014;**146**:277-282. DOI: 10.1016/j.matchemphys.2014.03.022

[33] Dan ZH, Qin FX, Yamaura S, Xie GQ, Makino A, Hara N. Refinement of nanoporous copper by dealloying MgCuY amorphous alloys in sulfuric acids containing polyvinylpyrrolidone. Journal of the Electrochemical Society. 2014;**161**:C120-C125. DOI: 10.1149/2.076403jes

[34] Thorp JC, Sieradzki K, Tang L, Crozier PA, Misra A, Nastasi M, Mitlin D, Picraux ST. Formation of nanoporous noble metal thin films by electrochemical dealloying of $Pt_xSi_{1-x}$. Applied Physics Letter. 2006;**88**:033110. DOI: 10.1063/1.2161939

[35] Wang XG, Qi Z, Zhao CC, Wang WM, Zhang ZH. Influence of alloy composition and dealloying solution on the formation and microstructure of monolithic nanoporous silver through chemical dealloying of Al-Ag alloys. The Journal of Physical Chemistry C. 2009;**113**:13139-13150. DOI: 10.1021/jp902490u

[36] Klement W, Willens RH, Duwez P. Non-crystalline structure in solidified gold-silicon alloys. Nature. 1960;**187**:869-870. DOI: 10.1038/187869b0

[37] Inoue A, Wang XM. Bulk amorphous FC20 (Fe-C-Si) alloys with small amounts of B and their crystallized structure and mechanical properties. Acta Materialia. 2000;**48**:1383-1395. DOI: 10.1016/S1359-6454(99)00394-8

[38] Ding Y, Kim YJ, Erlebacher J. Nanoporous gold leaf ancient technology. Advanced Materials. 2004;**16**:1897-1900. DOI: 10.1002/adma.200400792

[39] Kumar G, Singh DB, Tripathi VK. Surface enhanced Raman scattering of a surface plasma wave. Journal of Physics D: Applied Physics. 2006;**39**:4436-4439. DOI: 10.1088/0022-3727/39/20/021

[40] Tyson WR, Miller WA. Surface free energies of solid metals: Estimation from liquid surface tension measurements. Surface Science. 1977;**62**:267-276. DOI: 10.1016/0039-6028(77)90442-3

[41] Hakamada M, Mabuchi M. Preparation of nanoporous Ni and Ni-Cu by dealloying of rolled Ni-Mn and Ni-Cu-Mn alloys. Journal of Alloys and Compounds. 2009;**485**:583-587. DOI: 10.1016/j.jallcom.2009.06.031

[42] Dona JM, Gonzalez-Velasco J. Mechanism of surface diffusion of gold adatoms in contact with an electrolytic solution. The Journal of Physical Chemistry. 1993;**97**:4714-4719. DOI: 0022-3654/93/2097-47 14%04.00/

[43] Martienssen W, Warlimont H, editors. Springer Handbook of Condensed Matter and Materials Data. Springer Science & Business Media; 2006

[44] Ghosh G. Dissolution and interfacial reactions of thin-film Ti/Ni/Ag metallizations in solder joints. Acta Materialia. 2001;**49**:2609-2624. DOI: 10.1016/S1359-6454(01)00187-2

[45] Makin SM, Rowe AH, LeClaire AD. Self-diffusion in gold. Proceedings of the Physical Society. Section B. 1957;**70**:545-552. DOI: 10.1088/0370-1301/70/6/301

[46] Wang J, Liu HS, Liu LB, Jin ZP. Assessment of diffusion mobilities in FCC Cu-Ni alloys. Calphad. 2008;**32**:94-100. DOI: 10.1016/j.calphad.2007.08.001

[47] Wang CP, Yan LN, Han JJ, Liu XJ. Diffusion mobilities in the fcc Ag-Cu and Ag-Pd alloys. Calphad. 2012;**37**:57-64. DOI: 10.1016/j.calphad.2012.01.001

[48] Liu CL, Cohen JM, Adams JB, Voter AF. EAM study of surface self-diffusion of single adatoms of fee metals Ni, Cu, Al, Ag, Au, Pd, and Pt. Surface Science. 1991;**253**:334-344. DOI: 10.1016/0039-6028(91)90604-Q

[49] Samsonov GV. Handbook of the Physicochemical Properties of the Elements. Springer US; 1968

[50] Evangelakis GA, Kallinteris C, Papanicolaou NI. Molecular dynamics study of gold adatom diffusion on low-index copper surfaces. Surface Science. 1997;**394**:185-191. DOI: 10.1016/S0039-6028(97)00606-7

[51] Wang XD, Bednarcik J, Saksl K, Franz H, Cao QP, Jiang JZ. Tensile behavior of bulk metallic glasses by in situ X-ray diffraction. Applied Physics Letters. 2007;**081913**(1-3):91. DOI: 10.1063/1.2773945

[52] Wang XG, Sun JZ, Zhang C, Kou TY, Zhang ZH. On the microstructure, chemical composition, and porosity evolution of nanoporous alloy through successive dealloying of ternary Al-Pd-au precursor. The Journal of Physical Chemistry C. 2012;**116**:13271-13280. DOI: 10.1021/jp3035677